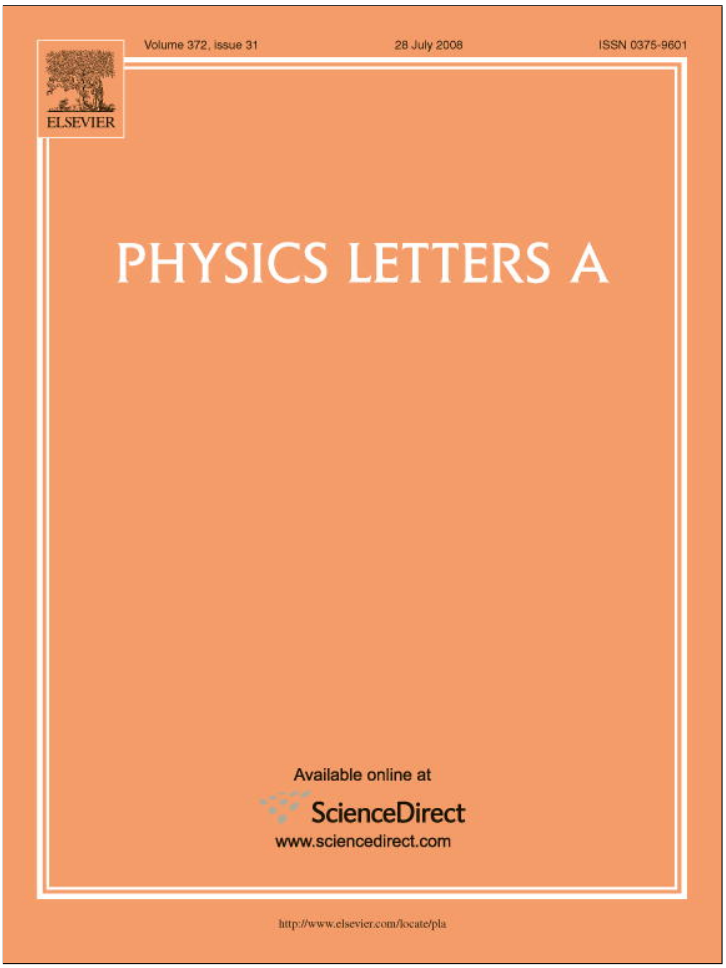

Physics Letters A 372 (2008) 5208–5214

Contents lists available at ScienceDirect

Physics Letters A

www.elsevier.com/locate/pla

Ordered structure formation in 2D mass asymmetric electron–hole plasmas

V.S. Filinov [a,*], H. Fehske [c], M. Bonitz [b], V.E. Fortov [a], P. Levashov [a]

[a] Institute for High Energy Density, Russian Academy of Sciences, Izhorskaya 13/19, Moscow 127412, Russia
[b] Christian-Albrechts-Universität zu Kiel, Institut für Theoretische Physik und Astrophysik, Leibnizstrasse 15, 24098 Kiel, Germany
[c] Institut für Physik, Ernst-Moritz-Arndt-Universität Greifswald, Felix-Hausdorff-Str. 6, D-17489 Greifswald, Germany

ARTICLE INFO

Article history:
Received 19 May 2008
Accepted 30 May 2008
Available online 5 June 2008
Communicated by V.M. Agranovich

PACS:
52.27.-h
52.25.-b

Keywords:
Ordered structures
Mass asymmetric two-dimensional dense plasmas

ABSTRACT

We study strong Coulomb correlations in dense two-dimensional electron–hole plasmas by means of direct path integral Monte Carlo simulations. In particular, the formation and dissociation of bound states, such as excitons, bi-excitons and many particle clusters, is analyzed and the density-temperature regions of their occurrence are identified. At high density, the Mott transition to the fully ionized state (electron–hole hexatic liquid) is detected. Particular attention is paid to the influence of the hole to electron mass ratio M on the properties of the plasma. For high enough values of M we observed the formation of Coulomb hole crystal-like structures.

1. Introduction

Strongly correlated two-dimensional Coulomb systems are the subject of intense recent research [1–11]. It is known that the competition between electrostatic and kinetic energy in an electron gas may be the reason of unusual phases of the electron system on a surface. The liquid state is stable when the kinetic energy dominates while the electrostatically favored "Wigner" triangular crystal is stable in opposite case [6]. In the region of interest, where there is a strong competition between the two kinds of energy, there may exist different phases. Instead of crystal-like long-range order in 2D systems there may exist phases with different asymptotic behavior of translation and orientation symmetry. Question under discussion is the existence of the anisotropic liquid phase (hexatic) intermediate between crystal and isotropic liquid and the nature of the transition between these phases. In classical case two possibilities are discussed. The first one is two stage topological melting with transition of crystal-like structure to hexatic liquid with short-range order (from power law translation order and long-range orientation order to the exponentially decaying translation pair distribution function and power law decaying of the orientation order). The second one is the transition of hexatic to isotropic liquid. The second possibility includes only one stage, namely, the first kind order transition of the crystal-like structure (power law translation order) to isotropic liquid. Appearance of the first kind transition is caused by the instability of the crystal lattice. It is possible that both scenarios can be realized.

In quantum case among the proposed intermediate phases between crystal and liquid there is a hexatic quantum phase [12,13]. Such phase would have orientational order, but no translational order. Another proposition is the presence of a supersolid phase, i.e. the quantum coexistence of the liquid with a crystal [14–16]. Around the melting point the system gains some energy for phase separation. However macroscopic phase separation is not possible as it would lead to a macroscopic dipole moment for a system with uniform neutralizing background. As consequence a series of microemulsion phases (bubbles/stripes of solid/liquid in the liquid/solid environment) have been suggested in [17,18]. Moreover an unexpected metal-insulator transition was discovered in the paper of Kravchenko et al. [19–21] but the origin of this transition is still under debate. In addition to the two already known phases (Fermi liquid at large density and Wigner crystal at low density) the authors of Refs. [22–24] discovered a third quantum stable phase at the intermediate values of density. This study of quantum melting of the two-dimensional Wigner crystal was made using a fixed node quantum Monte Carlo approach [25]. The third phase shows a hybrid behavior in between a liquid and a solid. In fixed node approximation this hybrid phase "with the symmetry of the crystal but liquid like properties" is more stable than both the liquid and the crystal phase. The liquid–hybrid transition takes place

* Corresponding author. Tel.: +7 495 931 07 19; fax: +7 495 485 79 90.
E-mail address: vladimir_filinov@mail.ru (V.S. Filinov).

0375-9601/$ – see front matter
doi:10.1016/j.physleta.2008.05.074

at $r_s = 31.5 \pm 0.5$. The hybrid phase has the nodal structure of a Slater determinant constructed out of the bands of a triangular lattice.

Let us note that the physical mechanism of melting can be influenced by the interaction with the substrate and defects. All the above mentioned possibilities for ordering phenomena in strongly correlated two-dimensional charged particle systems cause the necessity of first principle numerical simulations which are free from influence of the substrate and correctly can take into account quantum and statistical effects.

In our calculation we use the direct quantum path integral Monte Carlo method (PIMC) developed in our previous works for studying 3D strongly correlated two component plasma media such as hydrogen and electron–hole (e–h) plasmas at finite temperature. Here we present results for 2D e–h plasmas in a wide range of temperatures, densities and electron to hole mass ratios. Our calculations include the appearance and decay of bound states (excitons and biexcitons), the e–h plasma Mott transition from neutral system to metallic-like clusters, the formation of clusters in the hexatic-like liquid and the formation of a crystal-like lattice and, at very low temperatures, the transition of this 'lattice' to a state with antiferromagnetic structure. To present the complete phase diagram and comment on the problem of phase separation we need much more detailed calculations, however, which we are planned for subsequent work.

2. Path integral Monte Carlo approach

Let us consider a two-component neutral electron–hole plasma. Thermodynamic properties of a equilibrium electron–hole plasma are defined by the partition function Z, which for the case of N_e electrons and N_h holes ($N_e = N_h$) is given by

$$Z(N_e, N_h, V, \beta) = \frac{Q(N_e, N_h, \beta)}{N_e! N_h!}$$
$$\text{with } Q(N_e, N_h, \beta) = \sum_\sigma \int_V dr\, dq\, \rho(q, r, \sigma; \beta), \tag{1}$$

where $\beta = 1/k_B T$, $\sigma = (\sigma_e, \sigma_h)$, r, σ_e denote the space and spin electron coordinates $r_1, \ldots, r_{N_e}$ and $\sigma_1, \ldots, \sigma_{N_e}$, while q, σ_h refer to space and spin hole coordinates $q_1, \ldots, q_{N_h}$ and $\tilde{\sigma}_1, \ldots, \tilde{\sigma}_{N_h}$. The expressions are valid for 1D, 2D and 3D 'volumes' V if particle coordinates have related dimensionality.

The pair distribution functions for a binary mixture of quantum electrons and holes can be written in the form

$$g_{ab}(R_1 - R_2) = g_{ab}(R_1, R_2) = \frac{1}{Q(N_e, N_h, \beta)} \sum_\sigma \int_V dq\, dr\, \delta\big(R_1 - Q_1^a\big)\delta\big(R_2 - Q_2^b\big)\rho(q, r, \sigma, \beta), \tag{2}$$

where a and b label the particle species, i.e. $a, b = e$ (electrons), h (holes) and Q, R denote the two-dimensional vectors of the coordinates, $Q_{1,2}^e = r_{1,2}$ and $Q_{1,2}^h = q_{1,2}$.

The exact density matrixes of quantum systems for low temperature and high density is in general not known but can be constructed using a path integral representation [26] or operator identity $\rho = e^{-\beta\hat{H}} = e^{-\Delta\beta\hat{H}} \cdot e^{-\Delta\beta\hat{H}} \cdots e^{-\Delta\beta\hat{H}}$

$$\int_V dR^{(0)} \sum_\sigma \rho\big(R^{(0)}, \sigma; \beta\big) = \int_V dR^{(0)} \cdots dR^{(n)}\, \rho^{(1)} \cdot \rho^{(2)} \cdots \rho^{(n)} \times \sum_\sigma \sum_{P_e} \sum_{P_h} (\pm 1)^{\kappa_{P_e} + \kappa_{P_h}} \mathcal{S}(\sigma, \hat{P}_e \hat{P}_h \sigma') \hat{P}_e \hat{P}_h \rho^{(n+1)|}_{\sigma' = \sigma,\, R^{(n+1)} = R^{(0)}}, \tag{3}$$

where $\rho^{(i)} \equiv \rho(R^{(i-1)}, R^{(i)}; \Delta\beta) \equiv \langle R^{(i-1)}|e^{-\Delta\beta\hat{H}}|R^{(i)}\rangle$, and $\Delta\beta \equiv \beta/(n+1)$. $\hat{H}$ is the Hamilton operator, $\hat{H} = \hat{K} + \hat{U}_c$, containing kinetic and potential energy contributions, $\hat{K}$ and $\hat{U}_c$, respectively, with $\hat{U}_c = \hat{U}_c^h + \hat{U}_c^e + \hat{U}_c^{eh}$ being the sum of the Coulomb potentials (subscript c) between holes (superscript h), electrons (superscript e) and electrons and holes (superscript eh). Furthermore, $R^{(i)} = (q^{(i)}, r^{(i)}) \equiv (R_h^{(i)}, R_e^{(i)})$ is a $2(N_e + N_h)$ dimensional vector, index i denotes the high temperature ($(n+1)k_B T$) density matrixes $i = 1, \ldots, n+1$, $R^{(0)} \equiv (q, r) \equiv (R_h^{(0)}, R_e^{(0)})$, and $R^{(n+1)} \equiv R^{(0)}$ and $\sigma' = \sigma$. This means, each particle is represented by $(n+1)$ two-dimensional points called beads and the whole configuration of the particles is represented by a $2(N_e + N_h)(n+1)$ dimensional vector $[R] \equiv [R^{(0)}; R^{(1)}; \ldots; R^{(n)}; R^{(n+1)}]$. The spin gives rise to the spin part of the density matrix $\mathcal{S}$, whereas exchange effects are accounted for by the permutation operators $\hat{P}_e$ and $\hat{P}_h$, which act on the electron and hole coordinates $R^{(n+1)}$ and spin projections σ'. The sum is over all permutations with parity κ_{P_e} and κ_{P_h}.

An approximation for the high-temperature density matrix ρ_{sk} suitable for direct PIMC simulations has the form

$$\rho_{sk}\big([q], [r], \beta\big) = C_{N_e}^s C_{N_h}^k e^{-\beta U([q],[r],\beta)} \prod_{l=1}^{n} \prod_{p=1}^{N_e} \phi_{pp}^l \prod_{t=1}^{N_h} \tilde{\phi}_{tt}^l \det \big\| \psi_{ab}^{n,1} \big\|_{sk}, \tag{4}$$

where

$$U\big([q], [r], \beta\big) = \sum_{l=0}^{n} \big\{ U^e\big(r^{(l)}, \Delta\beta\big) + U^h\big(q^{(l)}, \Delta\beta\big) + U^{eh}\big(q^{(l)}, r^{(l)}, \Delta\beta\big) \big\}/(n+1). \tag{5}$$

Here we introduced dimensionless distances between neighboring beads—$\xi^{(1)}, \ldots, \xi^{(n)}$ and $\tilde{\xi}^{(1)}, \ldots, \tilde{\xi}^{(n)}$. More explicitly, $[r] \equiv [r; r + y_e^{(1)}; r + y_e^{(2)}; \ldots; r + y_e^{(n)}]$ and $[q] \equiv [q; q + \tilde{y}_h^{(1)}; q + \tilde{y}_h^{(2)}; \ldots; q + \tilde{y}_h^{(n)}]$, $\phi_{pp}^l \equiv \exp[-\pi|\xi_p^{(l)}|^2]$, $\tilde{\phi}_{tt}^l \equiv \exp[-\pi|\tilde{\xi}_t^{(l)}|^2]$ with $y_p^n = \Delta\lambda_e \sum_{k=1}^n \xi_p^{(k)}$ and $\tilde{y}_t^n = \Delta\lambda_h \sum_{k=1}^n \tilde{\xi}_t^{(k)}$, $\Delta\lambda_a^2 = 2\pi\hbar^2\Delta\beta/m_a$. The error of the above approximations for whole product on the r.h.s. of Eq. (3) is of the order $1/(n+1)$ [27]. Here U denotes the sum

$$U\big(R^{(i)}\big) = U^h\big(R_h^{(i)}\big) + U^e\big(R_e^{(i)}\big) + U^{eh}\big(R_h^{(i)}, R_e^{(i)}\big), \tag{6}$$

and U^h, U^e, U^{eh} are the pair sums of the off-diagonal two-particle effective potentials $\Phi^{ab}(\mathbf{r}_a, \mathbf{r}'_a, \mathbf{r}_b, \mathbf{r}'_b)$ [27]. The diagonal element ($\mathbf{r}'_a = \mathbf{r}_a$, $\mathbf{r}'_b = \mathbf{r}_b$) of Φ^{ab} is just the 2D analogue of the Kelbg potential, given by [28–30]

$$\Phi^{ab}\big(|\mathbf{r}_{ab}|, \Delta\beta\big) = \Phi^{ab}(\mathbf{r}_a, \mathbf{r}_a, \mathbf{r}_b, \mathbf{r}_b, \Delta\beta) = \frac{e_a e_b}{\lambda_{ab} x_{ab}} \big[1 - e^{-x_{ab}^2} + \sqrt{\pi} x_{ab} \big(1 - \mathrm{erf}(x_{ab})\big)\big], \tag{7}$$

where $x_{ab} = |\mathbf{r}_a - \mathbf{r}_b|/\lambda_{ab}$, and we underline that the Kelbg potential is finite at zero distance. The off-diagonal matrix elements of the effective binary potentials was approximated by the combination of the diagonal ones [27].

We underline that the density matrix (4) does not contain an explicit sum over the permutations and thus no sum of terms with

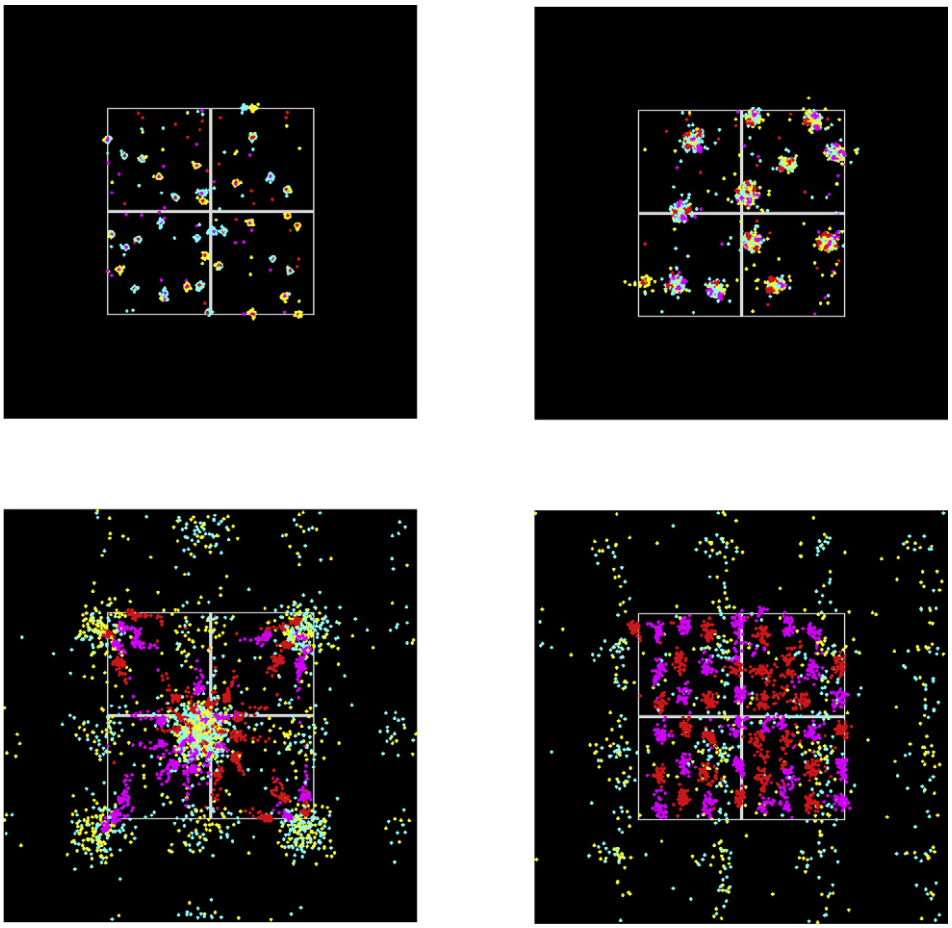

Fig. 1. (Color online.) Typical snapshots of particle configurations at different mass ratios, temperatures and densities. Upper left panel—$T/Ry = 0.045$, $r_s = 6$, the hole to electron mass ratio is $M = 800$, and the Monte Carlo cell size L is equal to $93a_B$; upper right one—$T/Ry = 0.007$, $r_s = 2$, $M = 200$ and $L = 31a_B$, lower left one—$T/Ry = 0.007$, $r_s = 0.5$, $M = 800$ and $L = 7.75a_B$; lower right one—$T/Ry = 0.007$, $r_s = 0.25$, $M = 800$ and $L = 3.87a_B$ respectively. Spin up and spin down electrons (holes) are marked by yellow and blue (red and pink) clouds of dots. The Monte Carlo cell is given by the gray grid lines.

alternating sign. Instead, the whole exchange problem is contained in a single determinant of the exchange matrix given by

$$\left\|\psi^{n,1}_{\alpha\gamma\zeta\eta}\right\|_{sk} \equiv \left\|e^{-\frac{\pi}{\Delta\lambda_e^2}|(r_\alpha - r_\gamma)+y^n_\alpha|^2}\right\|_s \cdot \left\|e^{-\frac{\pi}{\Delta\lambda_h^2}|(q_\zeta - q_\eta)+\tilde{y}^n_\zeta|^2}\right\|_k. \tag{8}$$

As a result of the spin summation, the matrix carries subscripts sk denoting the number of electrons and holes having the same spin projections. For more details, we refer to Ref. [31].

These expressions are well suited for efficient numerical evaluation using Monte Carlo techniques, e.g. [32,33]. In our Monte Carlo scheme we used different types of steps, where either electron r_i or hole q_i coordinates or individual electronic $\xi_i^{(k)}$ or hole $\tilde{\xi}_i^{(k)}$ beads, were moved until convergence of the calculated values was reached. To reduce the influence of the finite size effects we use for Monte Carlo cell the periodic boundary conditions (PBC). Our procedure has been extensively tested. In particular, we found from comparison with the known analytical expressions for pressure and energy of an ideal Fermi gas that the Fermi statistics is very well reproduced [34]. Further, we performed extensive tests for few-electron systems in a harmonic trap where, again, the analytically known limiting behavior (e.g. energies) is well reproduced [35,36]. For the present simulations of dense electron–hole plasma, we varied both the particle number and the number of beads. As a result we found that to obtain convergent results for the thermodynamic properties the particle numbers $N_e + N_h = 100$ and beads numbers in the range from $n = 20$ to $n = 40$ are adequate. To simplify the computations, we included only the dominant contribution in the sum over s, k corresponding to $s = N_e/2$ electrons and $k = N_h/2$ holes having spin up and down, respectively. The contribution of the other terms is small and vanishes in the thermodynamic limit. We should mention that for all obtained results, the maximum statistical error is about 5% and can be systematically reduced by increasing the length of the MC run.

3. Simulation results

We now apply the theoretical scheme developed in the preceding sections to a partially ionized two-dimensional dense e–h plasma. We will be interested in strong Coulomb correlation effects such as bound states (excitons, bi-excitons, many particle clusters), their modification by the surrounding plasma and their eventual breakup at high densities (Mott effect). Beyond the Mott density, we expect the possibility of hole crystallization if the hole mass is sufficiently large [37]. To detect these effects we extended our first-principle direct path integral Monte Carlo simulations to a large parameter space. Below, the density of the two-component plasma is characterized by the Brueckner parameter r_s defined as the ratio of the mean distance between particles $d = [\frac{1}{\pi(n_e+n_h)}]^{1/2}$ and the 3D exciton Bohr radius a_B, where n_e and n_h are electron and hole 2D densities. The dimensionless temperature will be presented as ratio of the temperature and 3D Rydberg, which includes reduced effective mass and dielectric constant. In what follows we compute and discuss the pair distribution functions, the spatial particle configurations, arising ordered e–h structures and transitions between them.

3.1. Particle configurations

In this section, we first present some spin-resolved typical "snapshots" of the electron–hole state in the simulation box for different particle densities, temperatures and electron to hole mass ratio (Fig. 1). According to the temperature decomposition of the density matrix, each electron and hole is represented by several tens of points ("beads") ($n = 20, \ldots, 40$). The spatial distribution of the beads of each quantum particle is proportional to its spatial probability distribution. Fig. 1 shows that in the case when the hole mass is much larger than the electron mass, the typical size of the cloud of beads for electrons is several times larger than the one for the holes. Note, that in the present strongly correlated system, the extension of electron and hole probability densities maybe quite different from the de Broglie wavelength which corresponds to the ideal case.

An interesting observation is that, at low temperature and low ($r_s = 10$, upper left panel) and intermediate densities ($r_s = 2$, upper right panel) practically all holes are closely covered by electron beads. From a physical point of view this means that electrons and holes form bound states, i.e. the electron–hole plasma consists mainly of excitons, bi-excitons and many-particle clusters, i.e. the electron–hole system is strongly inhomogeneous. In this case the mean distance between particles d is of the order of the electron wavelength. The existance of the bound states is also supported by the behavior of the pair distribution functions, exhibiting pronounced maxima at the distances of about half and a bit more of the Bohr radius (cf. the discussion in following section). We note that raising the temperature at fixed density leads to a (temperature-induced) ionization of the bound states. As a result we found a substantial number of free electrons and holes in the simulations (these simple snapshots are not included in this Letter).

From Fig. 1 it follows that growth of density results in increasing the particle number in the clusters. The structural analysis of large many particle clusters shows the hexagonal ordering of heavy holes (lower left panel). In this panel there are only two clusters: one is in the center of Monte Carlo cell, while the second one is divided on four parts (in each corner) due to periodic boundary conditions. Here besides the inner usual hexagonal structure the holes form filament-like structures at the border of the clusters. The filament-like structures are a 2D topological effect (for the 3D case the holes in analogous many-particles clusters have normal liquid-like ordering [38,39]).

If the particle density is high enough ($r_s = 0.25$) the electron wavelength becomes larger than the mean inter-particle distance d and even larger than the size of the Monte Carlo cell used in our simulations (see the large extension of the electron beads clouds). For $r_s \leqslant 0.5$ clusters become unstable because two electrons bound to neighboring holes start to overlap allowing for electron tunneling from one cluster to another. This means that bound states become unstable due to the Mott effect and the system transforms into a strongly correlated homogeneous electron–hole plasma. Since the hole wave-length is significantly smaller than the electron wavelength, it may still be smaller than d, in a certain region of r_s, and the structure of the hole beads resembles a liquid-like state. If the hole mass exceeds a critical value, the holes may even form a crystal-like structure [37] (lower right panel). The crystal-like ordering of the holes is accompanied by an oscillatory electron-density. At this very high density the type of the hole 'crystal' is clearly influenced by boundary conditions of Monte Carlo cell (finite size effect). So detailed analysis of the crystal-like structure should be done for a much larger number of particles in Monte Carlo cell.

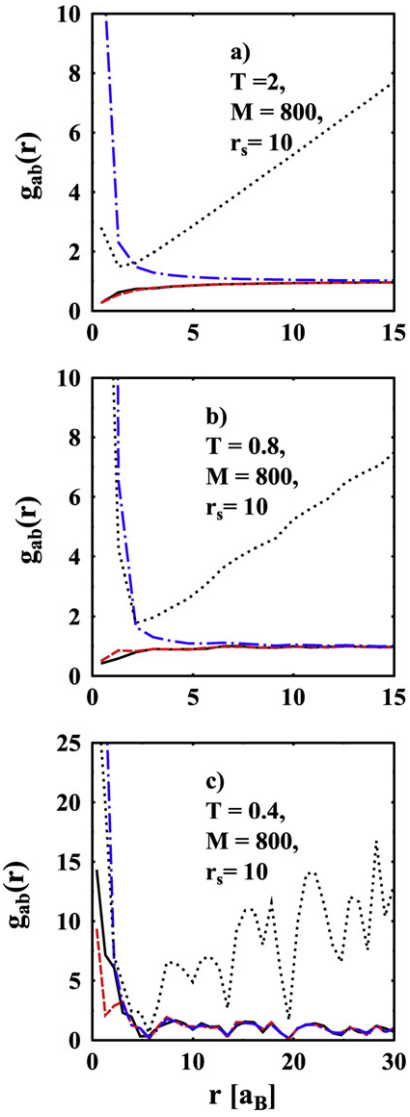

Fig. 2. (Color online.) Pair distribution functions g_{ee} (black solid line), g_{hh} (red dashed line), g_{eh} (blue dot-dashed line), $rg_{eh}/2$ (black dotted line) at density related to the Brueckner parameter $r_s = 10$, the hole to electron mass ratios M corresponding to $M = 800$ and three temperatures $T/Ry = 0.4$ (a), $T/Ry = 0.8$ (b), and $T/Ry = 2$ (c) respectively. The Monte Carlo cell size is equal to $155a_B$.

3.2. Pair distribution functions

At very high temperature and low density the electron–hole plasma consists of free electrons and holes. For free electrons and holes g_{ee} and g_{hh} are monotonically decreasing from one at large interparticle distances to zero at small distances due to Coulomb repulsion (see Fig. 2(a)). At the same time Coulomb attraction is the reason for sharp monotonic growth of g_{eh} with decreasing of the distance between electrons and holes (see Fig. 2(a)). The lowering of temperature at fixed density results in formation of two- and many-particle clusters. First appears two-particle clusters—excitons, then four-particle clusters—biexcitons and finally clusters with an increasing number of particles. This physical phenomenon is reflected in behavior of pair distribution functions (see Fig. 2). Formation of excitons is the reason for the very sharp growth of the g_{eh} at small distances and the maximum in the product $r * g_{eh}$ at distances of about half of one Bohr radius (Fig. 2(a), (b)). Formation of biexcitons can be seen by the appearance sharp peaks in the g_{hh} and g_{ee} pair distribution functions at the distances of the order of the Bohr radius (Fig. 2(c)). Due to the mass differ-

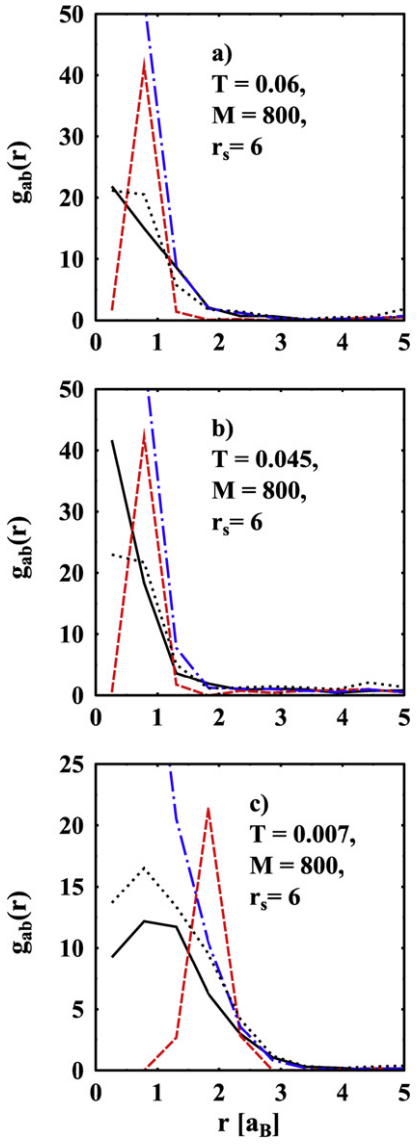

Fig. 3. (Color online.) Pair distribution functions g_{ee} (black solid line), g_{hh} (red dashed line), g_{eh} (blue dot-dashed line), $rg_{eh}/2$ (black dotted line) at hole to electron mass ratio $M = 800$, densities related to the Brueckner parameters $r_s = 6$ and three temperatures $T/Ry = 0.007$ (a), $T/Ry = 0.045$ (b) and $T/Ry = 0.06$ (c) respectively. The Monte Carlo cell size is equal to $93a_B$.

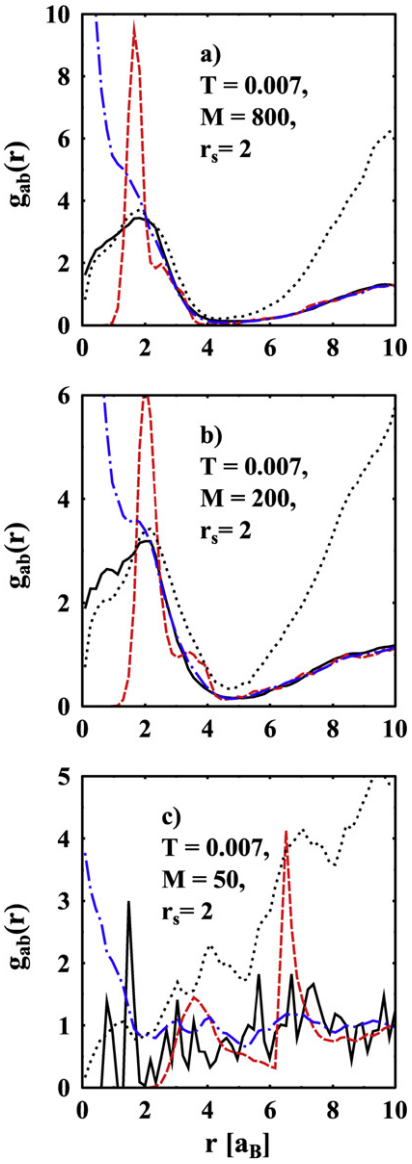

Fig. 4. (Color online.) Pair distribution functions g_{ee} (black solid line), g_{hh} (red dashed line), g_{eh} (blue dot-dashed line), $rg_{eh}/2$ (black dotted line) at temperature $T/Ry = 0.007$, density related to the Brueckner parameter $r_s = 2.0$, and hole to electron mass ratios $M = 800$ (a), $M = 200$ (b), and $M = 50$ (c) respectively. The Monte Carlo cell size is equal to $31a_B$.

ences of the electrons and holes the quantum effects due to the electron–electron interaction are more pronounced, whereas the repulsion between electron due to the tunneling effects is weaker (see Fig. 2(c)).

The formation of many-particle clusters and drops at lower temperatures results in broadening of the peaks and reduction of their height as can be seen from Figs. 3–5. More clearly the growth of the particle number in many particle clusters can be seen from Fig. 1. In Fig. 3(c) at the same e–h mass ratio and temperature as in Fig. 4(a) the height of the peaks of g_{hh} is smaller, while the width of the peaks is larger. The position of the peaks is shifted approximately by one Bohr radius in comparison with Fig. 3(a). So from Figs. 3 and 4 one can conclude that increasing the number of particles in many-particle cluster results in an enlargement of the hole–hole distances. The same tendency can be seen for the electron distances in clusters.

Increasing the number of particles in the clusters enhances the tendency towards a hexatic-like ordering of holes (Fig. 5(a)). This is reflected in the behavior of g_{hh} at high enough density. At the same time, a lowering of the density results in a reduction of the particle number within the clusters, destruction of the hole shell structure. Accordingly the peaks of the pair distribution functions g_{hh}, g_{ee} and g_{eh} grow (Fig. 5(b)). The behavior of these functions shows also the charge distribution inside the many-particle clusters and support the suggestion that the clusters should be electrically neutral.

A decrease of the hole mass from 800 to 50 results in more extended many-particle clusters (Fig. 4(c)) and the appearance of a well pronounced inner structure. The first peak of g_{hh} in Fig. 4(c) relates to holes with different spin projections, while the second one arises due to the Fermi repulsion between holes with the same spins. This finding is also supported by the analysis of the spin resolved pair correlation functions. The example of the spin resolved pair distribution function for $M = 800$ and $r_s = 0.25$ is given by Fig. 6. The figures presented before show the pair distribution functions averaged over the spin variables. Here we give an example for a spin resolved hole–hole pair distribution function g_{hh}

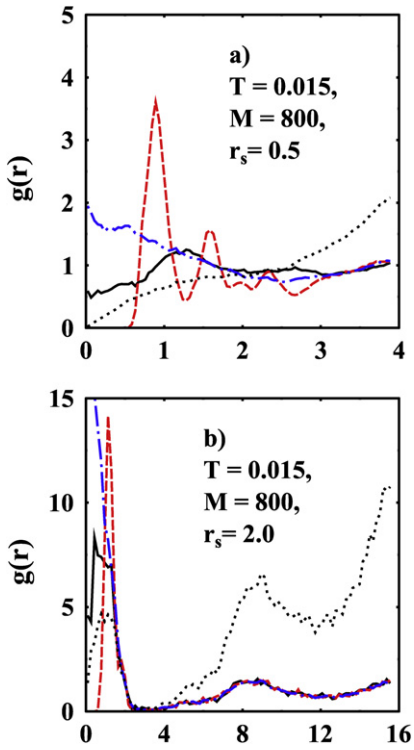

Fig. 5. (Color online.) Pair distribution functions g_{ee} (black solid line), g_{hh} (red dashed line), g_{eh} (blue dot-dashed line) at temperature $T/Ry = 0.015$, the hole to electron mass ratio $M = 800$, and two densities related to the Brueckner parameters $r_s = 0.5$ (a) and $r_s = 2.0$ (b) respectively.

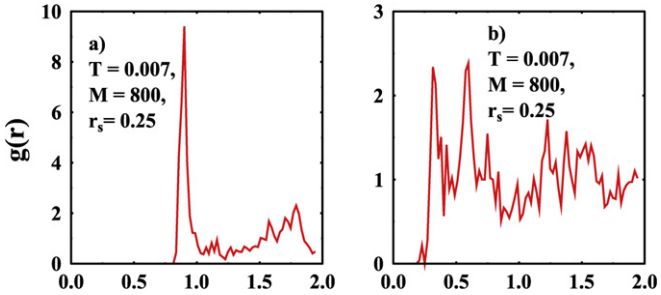

Fig. 6. (Color online.) Spin resolved pair distribution functions g_{hh} (red dashed line), at temperature $T/Ry = 0.007$, the hole to electron mass ratio $M = 800$, and a density related to the Brueckner parameter $r_s = 0.25$. Left (right) panel corresponds to parallel (antiparallel) hole spin projections.

related to crystal-like structures. Fig. 6(a) shows the short-range ordering of the holes due to the strong Fermi repulsion between holes with the same spin projections. So the holes with the same spin projection can form ordered crystal-like structures. Fermi repulsion does not exist between holes with different spin projections which is the physical reason for the different behavior of g_{hh} in Fig. 6(a) and (b), respectively. That is the ordering of the holes with different spin projection comes from the Coulomb repulsion which is weakened due tunneling effects. The result is that two crystal-like hole structures are immersed into each other.

4. Conclusion

In this Letter we have presented a computer simulation analysis of strong Coulomb correlations in dense two-dimensional two-component plasmas at low temperatures. In particular, the formation and dissociation of bound states, such as excitons, biexcitons and many particle clusters, is analyzed and the density-temperature region of their occurrence is identified. Particular attention is paid to the influence of the hole to electron mass ratio M on the properties of the plasma. From a plasma physics point of view these are very interesting systems because they allow to investigate nontrivial high-density effects of high current interest, such as the Mott effect and the plasma phase transition [38]. A theoretical treatment of these effects is very difficult, because quantum many-body effects such as bound state formation and screening have to be taken into account selfconsistently. While for such complex systems analytical methods fail, our first principle path integral Monte Carlo approach is well suited. In order to avoid additional approximations which are particularly questionable in the region of the Mott point, we used a direct fermionic simulations. With an improved treatment of the spin statistics we were able to present reliable simulations. Restricting the simulations to density values not significantly higher than the Mott density allowed us to avoid serious difficulties arising from the fermion sign problem. Within our scheme we have shown that, above the Mott point, a two-component plasmas with large mass anisotropy exhibits interesting Coulomb correlation phenomena: with increasing hole density it can undergo a phase transition to a Coulomb hexatic-like liquid and to a Wigner crystal (both are embedded in a degenerate electron gas). Note that the formation of crystal-like structures in a two-component plasma is possible for large enough mass ratios only [37].

Acknowledgement

This work has been supported by Deutsche Forschungsgemeinschaft through SFB TR-12. We thank Prof. Yu.E. Lozovik for fruitful discussions and made remarks.

References

[1] V.M. Bedanov, G.V. Gadijak, Yu.E. Lozovik, JETF 88 (1985) 1622.
[2] K.J. Stranburg, Rev. Mod. Phys. 60 (1988) 161.
[3] R.F. Morf, Helv. Phys. Acta 56 (1983) 743.
[4] A.F. Bakker, C. Bruin, H.J. Hilhorst, Phys. Rev. Lett. 52 (1984) 449.
[5] F.F. Abraham, Phys. Rep. 80 (1981) 339.
[6] M. Bonitz, et al., Phys. Plasmas 15 (2008) 055704.
[7] B.-J. Lin, L.-J. Chena, J. Chem. Phys. 126 (2007) 034706.
[8] X.H. Zheng, R. Grieve, Phys. Rev. B 73 (2006) 064205.
[9] C.H. Mak, Phys. Rev. E 73 (2006) 065104.
[10] S.Z. Lin, B. Zheng, S. Trimper, Phys. Rev. E 73 (2006) 066106.
[11] P. Keim, G. Maret, H.H. von Grunberg, Phys. Rev. E 75 (2007) 031402.
[12] V. Oganesyan, S.A. Kivelson, E. Fradkin, Phys. Rev. B 64 (2001) 195109.
[13] D.G. Barci, L.E. Oxman, Phys. Rev. B 67 (2003) 205108.
[14] B. Spivak, Phys. Rev. B 67 (2003) 125205.
[15] G. Katomeris, F. Silva, J.-L. Pichard, Eur. Phys. J. B 31 (2003) 401.
[16] Z.A. Nemeth, J.-L. Pichard, Eur. Phys. J. B 33 (2003) 87.
[17] R. Jamei, S. Kivelson, B. Spivak, Phys. Rev. Lett. 94 (2005) 056805.
[18] B. Spivak, S. Kivelson, Phys. Rev. B 70 (2004) 155114.
[19] S.V. Kravchenko, G.V. Kravchenko, J.E. Furneaux, V.M. Pudalov, M. D'Iorio, Phys. Rev. B 50 (1994) 8038.
[20] E. Abrahams, S.V. Kravchenko, M.P. Sarachik, Rev. Mod. Phys. 73 (2001) 251.
[21] S.V. Kravchenko, M.P. Sarachik, Rep. Prog. Phys. 67 (2004) 1.
[22] H. Falakshahi, X. Waintal, Phys. Rev. Lett. 94 (2005) 046801.
[23] X. Waintal, Phys. Rev. B 73 (2006) 075417.
[24] W.F. Vinen, C.J. Mellor, Phys. Scr. T 35 (1991) 145.
[25] B. Bernu, L.D. Candido, D.M. Ceperley, Phys. Rev. Lett. 86 (2001) 870.
[26] R.P. Feynman, A.R. Hibbs, Quantum Mechanics and Path Integrals, McGraw–Hill, New York, 1965.
[27] V.S. Filinov, High Temp. 13 (1975) 1065;
V.S. Filinov, High Temp. 14 (1976) 225.
[28] B.V. Zelener, G.E. Norman, V.S. Filinov, High Temp. 13 (1975) 650.
[29] G. Kelbg, Ann. Phys. 12 (1963) 219;
G. Kelbg, Ann. Phys. 13 (1964) 354;
G. Kelbg, Ann. Phys. 14 (1964) 394.
[30] W. Ebeling, H.J. Hoffmann, G. Kelbg, Contr. Plasma Phys. 7 (1967) 233, and references therein.
[31] V.S. Filinov, M. Bonitz, W. Ebeling, V.E. Fortov, Plasma Phys. Controlled Fusion 43 (2001) 743.
[32] V.M. Zamalin, G.E. Norman, V.S. Filinov, The Monte Carlo Method in Statistical Thermodynamics, Nauka, Moscow, 1977 (in Russian).

[33] K. Binder, G. Cicotti (Eds.), The Monte Carlo and Molecular Dynamics of Condensed Matter Systems, SIF, Bologna, 1996.
[34] V.S. Filinov, M. Bonitz, V.E. Fortov, JETP Lett. 72 (2000) 245.
[35] A.V. Filinov, Yu.E. Lozovik, M. Bonitz, Phys. Status Solidi B 221 (2000) 231.
[36] A.V. Filinov, M. Bonitz, Yu.E. Lozovik, Phys. Rev. Lett. 86 (2001) 3851.
[37] M. Bonitz, V.S. Filinov, V.E. Fortov, P.R. Levashov, H. Fehske, Phys. Rev. Lett. 95 (2005) 235006;
M. Bonitz, V.S. Filinov, V.E. Fortov, P.R. Levashov, H. Fehske, J. Phys. A 39 (2006) 4717.
[38] V.S. Filinov, V.E. Fortov, M. Bonitz, P.R. Levashov, JETF Lett. 74 (2001) 384, Pis'ma Zh. Eksp. Teor. Fiz. 74 (2001) 422.
[39] V.S. Filinov, M. Bonitz, V.E. Fortov, H. Fehske, P.R. Levashov, Phys. Status Solidi B 244 (2007) 474.